analytical chemistry

pubs.acs.org/ac Article

Colorimetric Detection of Nucleic Acids through Triplex-Hybridization Chain Reaction and DNA-Controlled Growth of Platinum Nanoparticles on Graphene Oxide

Weiwei Chen, Xiaobo Zhang, Juanjuan Li, Lizhen Chen, Ningning Wang, Siqi Yu, Guangming Li, Linfei Xiong, and Huangxian Ju*

Cite This: *Anal. Chem.* 2020, 92, 2714−2721 Read Online

ACCESS | Metrics & More | Article Recommendations | Supporting Information

ABSTRACT: The controllable growth of metal nanoparticles on nanomaterials is becoming a useful strategy for developing nanocomposites with designated performance. Here, a DNA-controlled strategy for growth of Pt nanoparticles on graphene oxide (GO−PtNPs) to regulate the nanozyme activity and a triplex-hybridization chain reaction (tHCR) for triggering the assembly of DNA probes to amplify the target-induced nanozyme catalytic signal were designed. The tHCR with one linear and two hairpin probes could be specially triggered by a tHCR trigger to form a long double-stranded DNA structure in the presence of target nucleic acid, which hindered the adsorption of these probes on a GO surface, and thus accelerated the growth of PtNPs. The formed GO−PtNPs showed strong catalytic activity toward the oxidation of 3,3,5,5-tetramethylbenzidine, thereby producing an amplified "turn-on" detection signal. The proposed method showed very high sensitivity with the detection limits down to 14.6 pM for mutant *KRAS* DNA and 21.7 pM for *let-7a* microRNA. This method was validated with better analytical performance than a general HCR system and could be effectively used for the identification of single-nucleotide polymorphisms, thus providing a novel approach for simple and sensitive detection of nucleic acids.

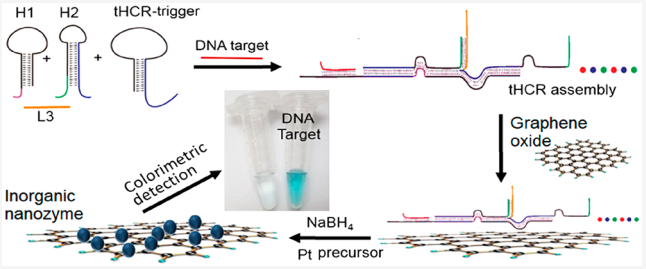

Inorganic nanomaterials have recently been widely applied for signal amplification in biosensing systems because of their unique structural design, easy interface functionalization, and controlled catalytic, optical, and electrical properties.[1−4] To endow these nanomaterials with desired recognition capability, research groups have modified various DNA structures on their surfaces.[5−7] Among these functionalization strategies, the self-assembly technique for forming highly ordered and stable composites has attracted considerable attention.[7−9] This noncovalent assembly is spontaneous without the formation or breaking of the chemical bond, which allows preservation of their intrinsic properties, such as the hybridization efficiency of DNA.[10−12] Moreover, the resulted composites possess the advantages of rapid signal response and simple preparation, suggesting wonderful application prospects in biosensing.[11−13]

Some inorganic nanomaterials have been used as nanozymes for the design of biosensing strategies,[14,15] which show more efficient properties, such as more rapid response to specific stimuli and better stability and controllability, than common proteases.[14,16,17] By self-assembly of DNA structure on the surface of inorganic nanomaterials, the catalytic capability of the formed nanozyme can be conveniently regulated,[18−21] which leads to several convenient, rapid, and economical colorimetric methods for detection of nucleic acids based on the different affinities of the nanomaterials to ssDNA and dsDNA.[16,20−24] However, the sensitivity of these methods is still limited because of the lack of efficient signal amplification strategy associated with the nanozyme-based colorimetric technology. Inspired by the efficient combination of hybridization chain reaction (HCR) with noncovalent interaction of DNA nanomaterials for improving the sensitivity of fluorescent detection,[25,26] this work attempted to design an HCR-controlled inorganic nanozyme for highly sensitive colorimetric detection.

The typical HCR contains two kinds of assembly probes: linear type and hairpin type.[25,27,28] The linear-type DNA chains possess higher affinity to inorganic nanomaterials. However, the assembly of linear chains lacks the specificity enough for highly selective biosensing of nucleic acids. The cross-opening of two DNA hairpins triggered by a target initiator provides an alternation for specific HCR. But the hairpin-type structure possesses less affinity for its absorption on a nanomaterial surface because of the presence of long

Received: October 28, 2019
Accepted: January 8, 2020
Published: January 8, 2020

https://dx.doi.org/10.1021/acs.analchem.9b04909
Anal. Chem. 2020, 92, 2714−2721

complementary sequences to form the double-stranded stem. Thus, this work integrated both the strong absorption of a linear-type DNA chain and the high specificity of a hairpin-type structure to design a triplex-hybridization chain reaction (tHCR) for triggering the assembly of DNA strands and improving both the sensitivity and the selectivity of target nucleic acid controlled nanozyme colorimetric assay.

The designed tHCR was triggered by a DNA trigger in the presence of one linear and two hairpin probes. To achieve target nucleic acid detection, here, we designed a tHCR trigger to recognize the target nucleic acid for the formation of a single-strand sequence to serve as the DNA trigger (Scheme 1). Because of the tremendous surface area, amphiphilicity,[29,30]

Scheme 1. Schematic Illustration of Colorimetric Strategy for Detection of Nucleic Acids by Integrating tHCR and DNA-Controlled Growth of PtNPs on GO

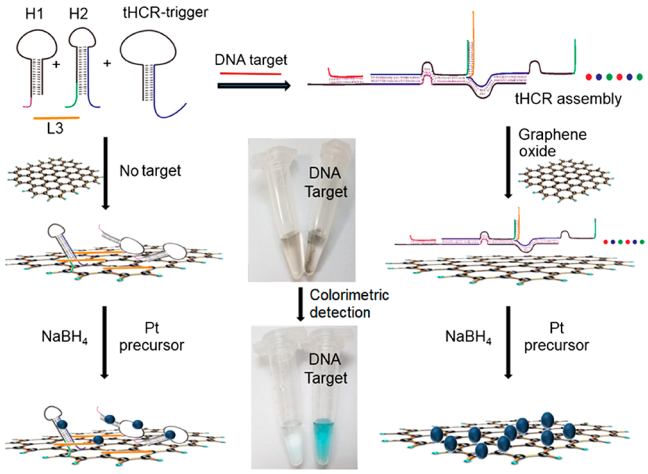

and different affinities to ssDNA and dsDNA, graphene oxide (GO) was used as a support for the formation of an inorganic nanozyme by in situ growth of Pt nanoparticles (PtNPs) on its surface. The presence of three probes hindered the growth of PtNPs because of their adsorption on the GO surface, and little DNA-doped GO–PtNPs (GO/DNA–PtNPs) possessed very low nanozyme activity. In contrast, target-induced tHCR assembly formed a long double-stranded DNA structure, which hindered the adsorption of these probes on the GO surface, and thus accelerated the growth of PtNPs. Thus, the target nucleic acid could regulate the nanozyme activity, leading to a colorimetric strategy for nucleic acid detection. The tHCR amplified colorimetric method showed excellent performance for detection of both DNA and microRNA (miR), indicating its good expansibility and promising application in bioassays.

EXPERIMENTAL SECTION

Materials and Reagents. Sodium borohydride ($NaBH_4$), 3,3,5,5-tetramethylbenzidine (TMB), 2-(morpholino)-ethanesulfonic acid monohydrate (MES), and potassium tetrachloroplatinate(II) (K_2PtCl_4) were purchased from Sigma. TMB/H_2O_2 colorimetric substrate solution consisted of 2% v/v TMB (20 mM), H_2O_2 (30% w/w), and 140 mM sodium acetate in 20 mM MES–acetate buffer (pH 4.0). Phosphate buffered saline (PBS, pH 7.4) and Tris-acetate-ethylenediaminetetraacetic acid (TAE) buffer was obtained from Solarbio Company. Tris-HCl buffer (1 M) was obtained from Sangon Biotech Co., Ltd. (Shanghai, China). Graphene oxide was obtained from Nanjing NFNANO Company. All DNA oligonucleotides and miRNAs (Table S1, Supporting Information) were purchased from Sangon Biotech Co., Ltd. (Shanghai, China). Twenty millimolar Tris-HCl buffer (pH 7.4) containing 140 mM NaCl and 5 mM $MgCl_2$ was used as tHCR running buffer. All oligonucleotides and reagents were dissolved in Ultrapure DNase/RNase-Free Distilled Water and stored at −20 °C.

Apparatus. The scanning electron microscope (SEM) and transmission electron microscope (TEM) images were obtained on a S-7800 scanning electron microscope (Hitachi, Japan) and a JEM-2100 transmission electron microscope (JEOL Ltd., Japan), respectively. Absorption spectra were recorded with a UV-3600 UV–vis–NIR spectrophotometer (Shimadzu). Infrared spectra were recorded on a Vector 22 Fourier transform infrared (FT-IR) spectrometer (Bruker Optics, Germany). Dynamic light scattering (DLS) measurement was performed on a 90 Plus/BI-MAS equipment (Brookhaven Instruments).

Synthesis of GO–PtNPs and GO/DNA–PtNPs. The process to prepare GO/DNA–PtNPs was as follows: first, 6 μL of GO dispersion (1 mg mL^{-1}) and 5 μL of 100 μM linear DNA were mixed in 90 μL of 20 mM Tris-HCl buffer. After the mixture was kept at room temperature for 45 min with oscillation mixing every 15 min, the linear DNA could strongly adsorb on the GO surface through strong π–π interaction. The GO/DNA was collected by centrifugation (6000 rpm, 1 min), washed with Tris-HCl buffer, and redispersed in 100 μL of 10 mM PBS. The in situ growth of PtNPs was carried out through addition of 15 μL of $NaBH_4$ (5 mM) in 100 μL of GO/DNA dispersion containing 1.5 μM K_2PtCl_4 to react for 5 min at room temperature (RT).[18] The GO–PtNPs were synthesized in the absence of DNA.

Colorimetric Analysis of Nucleic Acids. Before the tHCR assembly, tHCR-trigger, H1, and H2 were heated to 95 °C for 5 min and then allowed to cool to room temperature for 3 h. Then 5 μL of H1, H2, and L3 (10 μM) and tHCR-trigger (3.0 μM) were individually mixed into 80 μL of tHCR running buffer containing 60 μg mL^{-1} GO and target nucleic acid with different concentrations to incubate at 4 °C for 2 h. Afterward, the nanomaterials were collected by centrifugation (6000 rpm, 1 min), washed with Tris-HCl buffer to remove the residual reactants, and redispersed in 100 μL of 10 mM PBS containing 1.5 μM K_2PtCl_4. Then 15 μL of $NaBH_4$ (5 mM) was added into this dispersion to react for 5 min at RT. After the product was collected by centrifugation (6000 rpm, 1 min) and washed with PBS, it was dispersed in 200 μL of TMB/H_2O_2 substrate solution to incubate for 3 min at RT. Upon addition of 4 M H_2SO_4 (200 μL) to stop the reaction, the solution color changed from blue to yellow. The mixture was then diluted to 800 μL to record the UV absorption spectrum.

RESULTS AND DISCUSSION

Design of the tHCR System and GO–PtNPs Nanozyme for Colorimetric Assay of Nucleic Acids. The tHCR contained one linear probe (L3) and two hairpin probes (H1 and H2) as illustrated in Scheme S1A. In the presence of DNA trigger, H2 was first opened to hybridize with H1 from the pink end and then L3 in the green part (Table S1), and another end of opened H1 continued to open H2, which led to the cyclic assembly of H1, H2, and L3. The cyclic tHCR produced a long double-stranded DNA structure. For increased structure stability, the H1 loop contained 12 bases

https://dx.doi.org/10.1021/acs.analchem.9b04909
Anal. Chem. 2020, 92, 2714–2721

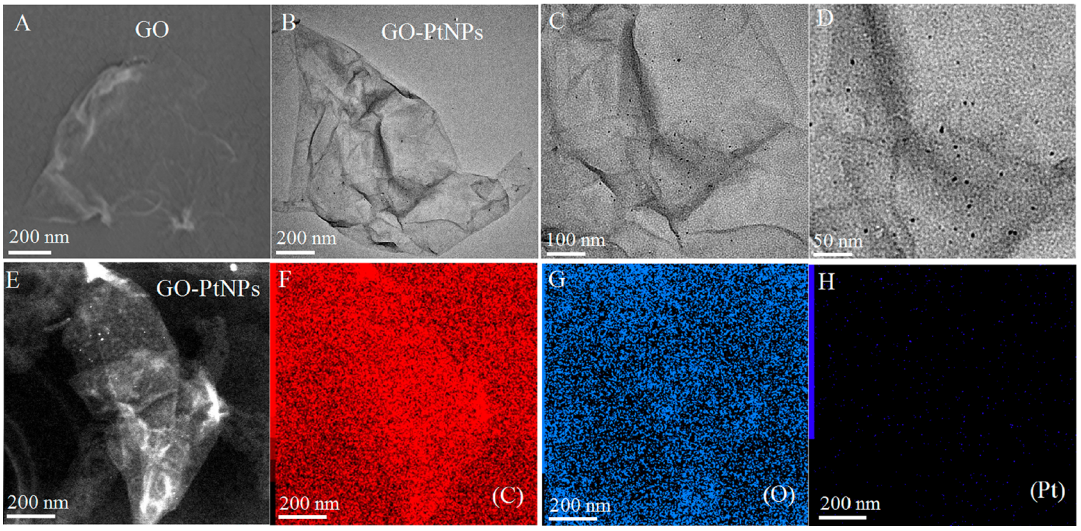

Figure 1. (A) SEM image of GO, (B–D) TEM images of GO–PtNPs at different magnifications, (E) dark-field scanning TEM (STEM), and (F–H) X-ray energy-dispersive spectroscopic (EDS) elemental mapping images of C (F), O (G), and Pt (H) for GO–PtNPs.

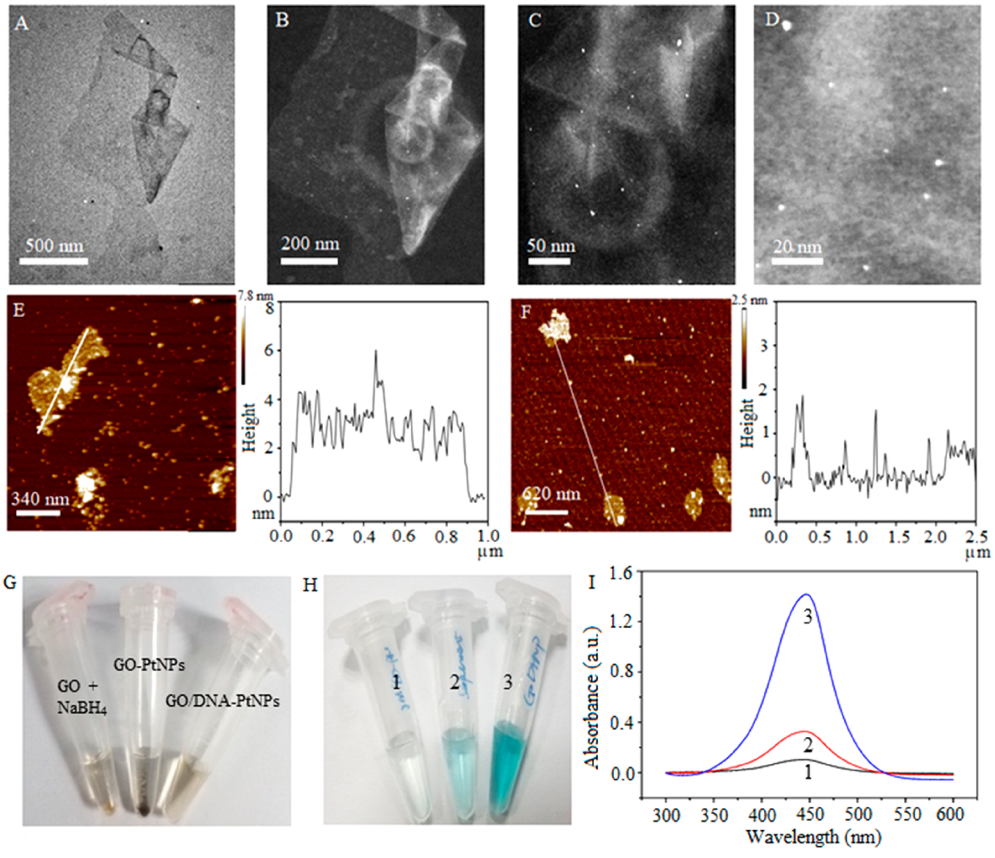

Figure 2. (A) TEM and (B–D) STEM images of GO/DNA–PtNPs. (E, F) Typical AFM images and height profiles of GO–PtNPs (E) and DNA/GO–PtNPs (F) on a mica substrate. (G) Photographs of $NaBH_4$-reduced GO, GO–PtNPs, and GO/DNA–PtNPs. (H, I) Photographs and UV–vis spectra of TMB and H_2O_2 in the presence of (1) precipitates of GO/DNA–PtNPs, (2) supernatant of DNA/GO–PtNPs, and (3) precipitates of GO–PtNPs.

(underlined in Table S1), which formed an arched double strand upon hybridization with the 3′ end of H2. To avoid the spontaneous hybridization of L3 with the 5′ end of H2, we embedded 6 bases complementary to L3 in the H2 stem. To achieve the detection of target nucleic acids, we designed a target sequence-dependent tHCR trigger with the hairpin-type structure to recognize the target nucleic acid. As shown in Scheme S1B, the recognition opened the tHCR trigger for exposure of the single-stranded sequence to hybridize with H2, which triggered the cyclic assembly of H1, H2, and L3 (Scheme S1C). The loop of the tHCR trigger contained 20 bases, and 18 of them were complementary to the target sequence; thus, their recognition could open the tHCR trigger

https://dx.doi.org/10.1021/acs.analchem.9b04909
Anal. Chem. 2020, 92, 2714–2721

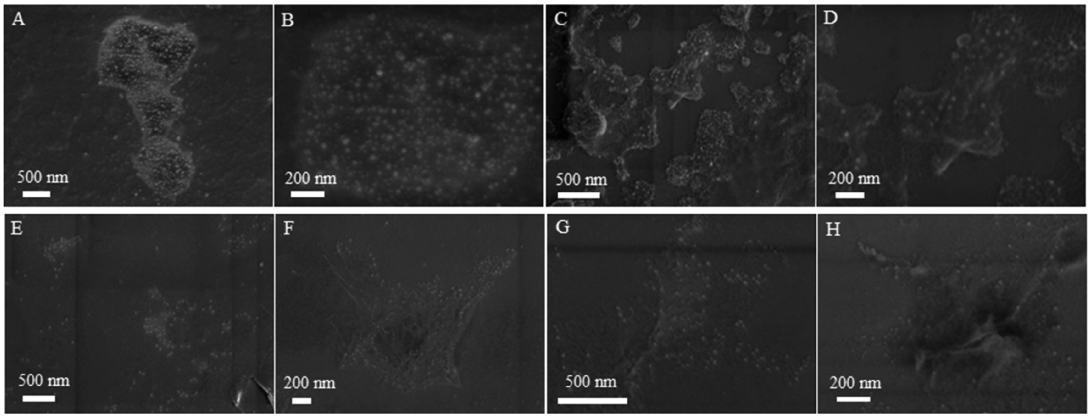

Figure 3. SEM images of GO−PtNPs grown on GO at 0.65 mM $NaBH_4$ and (A, B) 2.0 and (C, D) 0.5 μM Pt precursor, and GO/DNA−PtNPs grown at 5 μM linear DNA, 0.65 mM $NaBH_4$, and (E, F) 2.0 and (G, H) 0.5 μM Pt precursor under different magnifications.

because of the significantly longer sequence compared to the stem with 10-base pairs.

Through the tHCR, the deposition of PtNPs on the GO surface in the presence of K_2PtCl_4 and the reducing agent ($NaBH_4$) could be efficiently controlled. In the absence of target, the three free probes could adsorb on GO via the $\pi-\pi$ stacking interaction, which hindered the deposition of PtNPs (Scheme 1). Because of the incomplete coverage, little DNA-doped GO−PtNPs (GO/DNA−PtNPs) could be formed on the surface, but they possessed very low nanozyme activity. Upon the tHCR in the presence of target nucleic acid, the formed double-stranded DNA structure hindered the adsorption of these probes on the GO surface, and thus accelerated the growth of PtNPs to form highly active GO−PtNPs nanozyme for catalyzing the oxidation of 3,3,5,5-tetramethylbenzidine (TMB), leading to an amplified colorimetric method for detection of target nucleic acids.

Effect of DNA Adsorption on GO Surface on Growth of PtNPs. The deposition of PtNPs on the GO surface was performed by simply adding K_2PtCl_4 and $NaBH_4$ in GO dispersion. The GO showed a two-dimensional (2D) sheet morphology with some raised folds in the margin (Figure 1A). After the PtNPs were deposited on its surface, the TEM and STEM images showed monodispersed PtNPs with an average size of 6 nm decorated on GO (Figure 1B−E). The elemental mapping further revealed the uniform distribution of C, O, and Pt atoms in the GO support (Figure 1F−H). The field emission SEM (FESEM) elemental mapping and X-ray energy-dispersive spectrum further verified the composition of GO−PtNPs (Figure S1).

In the presence of linear DNA, the adsorption of DNA on the GO surface hindered the growth of PtNPs; thus, the TEM and STEM images of the formed GO/DNA−PtNPs showed sparsely distributed PtNPs with smaller size (1−2 nm) (Figure 2A−D), which led to less height of the AFM image (Figure 2E,F) and much smaller DLS diameter (Figure S2A,B) than that of GO−PtNPs. Generally, the thermodynamic stability of small-sized NPs was low; the presence of smaller PtNPs indicated higher surface energy on DNA-adsorbed GO.[14,18] Thus, DNA played an important role in regulating the growth of PtNPs.

After $NaBH_4$ was added into the GO dispersion, some yellow precipitates were observed (Figure 2G), which resulted from the reduction of oxygen groups of the GO surface to decrease the dispersion and increase the DLS diameter (Figure S2C,D). Thus, the GO surface could be partly reduced by $NaBH_4$ during the reductive deposition of PtNPs on GO or GO/DNA, which led to the increase of band−intensity ratio of D (1350 cm^{-1}) to G (1590 cm^{-1}) peaks from 0.68 to 0.82 or 0.73 in Raman spectra (Figure S3).[31,32] The lower increase for GO/DNA indicated the effect of absorbed DNA on the reduction of GO. Furthermore, the formed GO/DNA−PtNPs showed better dispersibility than GO−PtNPs (Figure 2G).

The growth of PtNPs on GO also depended on the concentrations of Pt precursor. With the increasing concentration of K_2PtCl_4, more PtNPs were formed on the GO surface (Figure 3A−D), which led to the aggregation and the decreased dispersibility of the GO−PtNPs; thus, the DLS diameter of obtained GO−PtNPs increased (Figure S4). At low K_2PtCl_4 concentration, the SEM images of GO−PtNPs showed more raised folds, whereas high K_2PtCl_4 concentration alternated the natural state of GO. However, the adsorption of DNA on GO could keep the folds upon the deposition of PtNPs at different Pt precursor concentrations because of the relatively slow deposition rate (Figure 3E−H), which confirmed the controllable growth of PtNPs.

Regulation of DNA on Nanozyme Activity of GO−PtNPs. The nanozyme activities of GO−PtNPs and DNA/GO−PtNPs were studied by their catalysis toward the oxidation of TMB by H_2O_2. Upon addition of GO−PtNPs dispersion in the mixture of TMB and H_2O_2, the solution color changed remarkably to blue (Figure 2H), and the corresponding UV−vis spectrum showed the maximum absorbance at 450 nm (Figure 2I), which was attributed to the oxidation product of TMB, suggesting the good peroxidase activity of GO−PtNPs. In the absence of PtNPs, the addition of both GO and $NaBH_4$-reduced GO did not show any change (not shown). Moreover, the addition of GO/DNA−PtNPs precipitates produced little change in solution color and very low absorbance of the oxidation product. After the supernatant of DNA/GO−PtNPs was incubated with the mixture of TMB/H_2O_2, both the solution color and the UV−vis spectrum showed distinguishable change because of the good dispersibility of GO/DNA−PtNPs. But the adsorption peak was much weaker than that in the presence of GO−PtNPs (Figure 2I), indicating much lower nanozyme activity. Thus, the adsorbed DNA regulated not only the growth of PtNPs but also the nanozyme activity of the formed nanocomposites, which led to a strategy for design of the colorimetric detection methods based on the different affinities of GO to ssDNA and dsDNA.

https://dx.doi.org/10.1021/acs.analchem.9b04909
Anal. Chem. 2020, 92, 2714−2721

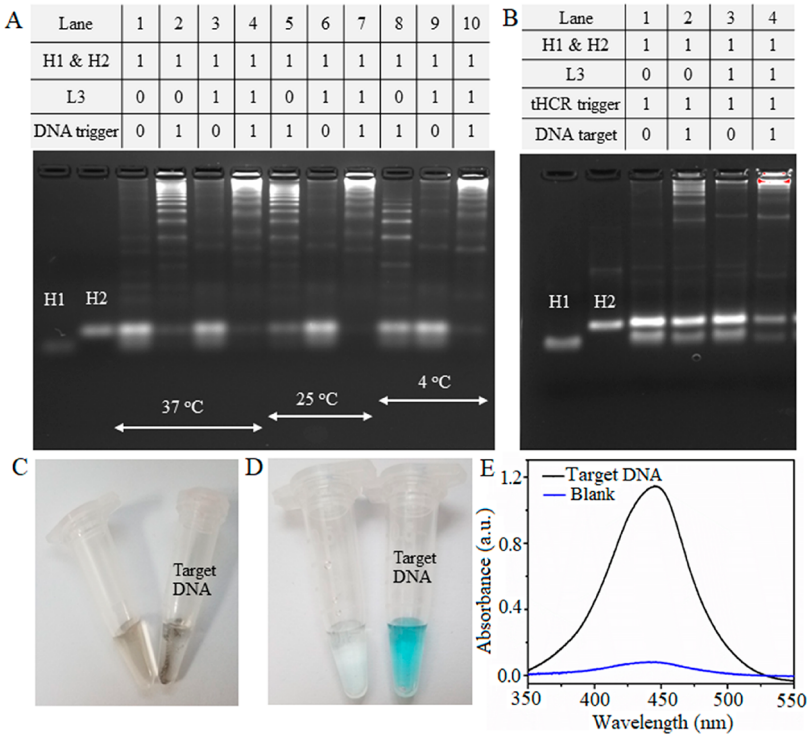

Figure 4. Gel electrophoresis of different mixtures for validating the feasibility of tHCR triggered by (A) DNA trigger at 37, 25, and 4 °C and (B) target DNA and tHCR-trigger at 4 °C. (C) Photographs of centrifuged precipitates formed by deposition of PtNPs on GO in tHCR solution without (left) and with target *KRAS* gene (right). (D,E) Photographs and UV−vis spectra of TMB and H_2O_2 in the presence of (C).

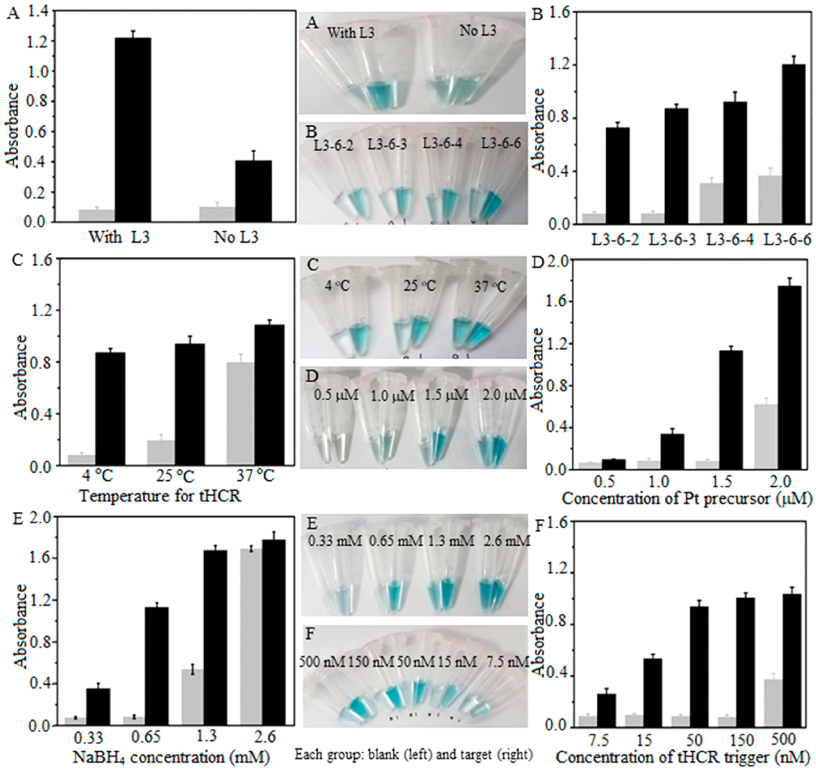

Figure 5. (A) Absorbance of detection solution in the presence and absence of L3. (B−F) Effects of L3 sequence (B), tHCR temperature (C), Pt precursor concentration (D), $NaBH_4$ concentration (E), and tHCR-trigger concentration (F) on the response of 0.05 μM DNA at the incubation time of 1 h and other optimized conditions. Gray and black represent blank and target groups.

Colorimetric Assay by Integrating tHCR with GO−PtNPs Nanozyme. The designed tHCR was first confirmed with agarose gel electrophoresis. As shown in Figure 4A, in the absence of DNA trigger Lane 1 showed only the bands of H1 and H2, which disappeared upon addition of DNA trigger at 37 °C (Lane 2), indicating the general HCR. The addition of

https://dx.doi.org/10.1021/acs.analchem.9b04909
Anal. Chem. 2020, 92, 2714−2721

L3 in the mixture of H1 and H2 did not affect their bands (Lane 3), excluding the spontaneous assembly among H1, H2, and L3 (Lanes 3, 6, and 9). But further addition of DNA trigger in the mixture led to both the disappearance of these probe bands and slightly higher molecular weight of the product (Lane 4) than that in the absence of L3, indicating the hybridization of L3 with the green part of H2 to achieve the tHCR. With the decreasing reaction temperature, the HCR became slower, which led to weakened brightness of the HCR product and enhanced bands of H1 and H2 (Lanes 2, 5, and 8). However, the temperature showed less influence on tHCR, which resulted in similar bands at different temperatures (Lanes 4, 7, and 10). Thus, the presence of L3 greatly improved the HCR rate and the stability of the tHCR product.

To achieve the specific detection of target nucleic acids, we replaced the DNA trigger with target DNA (mutant *KRAS* gene) and a designed tHCR trigger. In the absence of target DNA, the addition of tHCR trigger did not produce obvious assembly of H1, H2, and L3 (Figure 4B, Lanes 1 and 3). When the mixture of the target DNA and tHCR trigger was added to the solution of H1 and H2, the HCR was also unobvious at 4 °C because of the slow reaction rate in the absence of L3 (Figure 4B, Lane 2). In contrast, the bands of H1 and H2 obviously weakened, and the bright band of the assembly product occurred after the mixture of H1, H2, L3, target DNA, and tHCR trigger was incubated for 2 h (Figure 4B, Lane 4), demonstrating the target DNA-triggered tHCR.

To confirm the feasibility of tHCR amplified colorimetric detection, we mixed the tHCR system with GO dispersion to deposit PtNPs on the GO surface, and the formed precipitates were centrifuged to catalyze the oxidation of TMB by H_2O_2. Upon the addition of target DNA in the tHCR system, the GO−PtNPs with high nanozyme activity could be formed, which led to observable precipitates and obvious color change of TMB/H_2O_2 solution (Figure 4C,D). The absence of target DNA greatly weakened the color change because of the adsorption of these tHCR probes on GO to hinder the deposition of PtNPs, which led to negligible absorbance response (Figure 4E). The significant color or absorbance change demonstrated a highly sensitive colorimetric method for detection of target DNA.

Optimization of Detection Conditions. The necessity of the L3 probe for amplified colorimetric detection was first demonstrated. At the target DNA concentration of 50 nM, the detection solution showed the absorbance of 1.23 along with a background value of 0.08, which was detected in a blank solution, in the presence of 0.5 μM L3, whereas they were 0.39 and 0.10 in the absence of L3 (Figure 5A). Thus, the tHCR increased the ratio of signal to background by 3.94 times, indicating the improved sensitivity. To achieve the excellent biosensing performance and exclude the spontaneous assembly among the three probes, the number of bases complementary to the 5′ end of H2 in the L3 probe was also optimized at 4 °C using mutant *KRAS* gene as DNA target. Compared to L3−6−6, L3−6−4, and L3−6−2 (Table S1), L3−6−3 gave the maximum ratio of signal to background (Figure 5B). More L3 bases complementary to the 5′ end of H2 could open H2 to produce spontaneous assembly and high background. Therefore, L3−6−3 was chosen as the optimum sequence for subsequent experiments.

As mentioned above, the presence of L3 accelerated the HCR and the assembly of DNA probes. Thus, the spontaneous assembly in the absence of target DNA could be observed at relatively higher incubation temperature (Figure S5), which could bring high background. As shown in Figure 5C, with the increasing tHCR temperature, the ratio of signal to background decreased greatly. The background almost approached the response signal at 37 °C. Thus, for subsequent experiments, 4 °C was selected for tHCR.

The concentrations of Pt precursor and $NaBH_4$ also showed obvious effects on the ratio of signal to background (Figure 5D,E). When they were larger than 1.5 μM and 0.65 mM, respectively, the background became larger. This suggested that 1.5 μM Pt precursor and 0.65 mM $NaBH_4$ were the optimal conditions for reductive deposition of PtNPs on GO to perform the nanozyme-catalyzed colorimetric detection of target DNA.

Lastly, with the increasing concentration of tHCR trigger, the absorbance signal increased gradually and then trended to the maximum value at concentrations higher than 50 nM, whereas the background signal stayed at the same value up to 150 nM (Figure 5F). Therefore, 150 nM of the HCR-trigger was used for subsequent colorimetric detections.

Analytical Performance for *KRAS* Gene Detection. It is generally known that genetic alternation plays important roles in the occurrence of malignant tumors. Among these gene mutations, the *KRAS* mutation is one of the most frequently mutated genes that have been identified in various cancers.[33] Thus, there is an eager need to develop detection methods for *KRAS* mutation. Herein, the designed strategy integrating target-triggered tHCR and DNA-controlled growth of PtNPs on GO was used for nanozyme-catalyzed colorimetric detection of mutant *KRAS* gene under optimized conditions. As shown in Figure 6A, the color of the detection solution became bluer with the increasing *KRAS* DNA concentration, indicating more GO−PtNPs were produced because of the formation of long double-stranded tHCR assemblies, which hindered the adsorption of DNA probes on the GO surface. Correspondingly, the UV−vis spectra showed increased absorbance (Figure 6B), and the plot of absorbance at 450 nm versus target concentration trended to a maximum value at high DNA concentration (Figure 6C). Interestingly, the plot of absorbance versus the logarithm value of DNA concentration showed a linearity ranging from 25 pM to 5.0 nM (R = 0.992, Figure 6D). The limit of detection (LOD) was 14.6 pM, calculated from the linear slope and 3σ of the blank signal. Compared with previous colorimetric methods based on DNA−inorganic nanomaterials, the LOD was 34 times lower than the lowest value (Table S2), indicating the high sensitivity of the proposed method.

The selectivity of the *KRAS* detection system was validated by comparing the response with those of wild *KRAS* (single-base mismatch), two-bases mismatch, three-bases mismatch, and noncomplementary DNA. As shown in Figure 6E,F, three-bases mismatch and noncomplementary DNA showed negligible response, and the response for two-bases mismatch was also not significant. The wild *KRAS* DNA showed significantly lower response than the target, suggesting good SNP discrimination capability and high specificity.

Detection of MicroRNA. MicroRNA is a short, noncoding single-stranded RNA that has been considered an important tumor marker, and the aberrant expression of microRNA is highly associated with cancer type and stage.[34] Considering the significance of microRNA (miR) in early cancer diagnostic and prognostic processes, we further used *let-7a* miR as a target to design the tHCR trigger for examining the practicability of this

https://dx.doi.org/10.1021/acs.analchem.9b04909
Anal. Chem. 2020, 92, 2714−2721

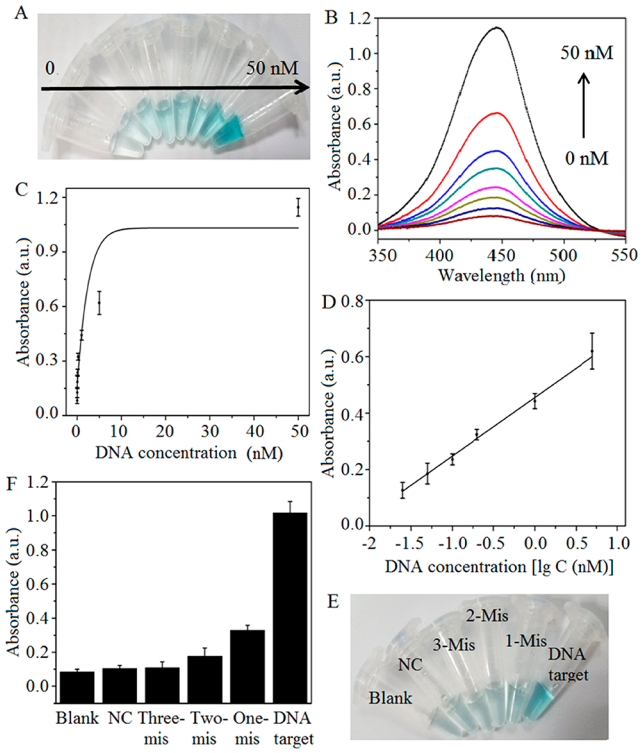

Figure 6. (A) Photograph and (B) UV−vis spectra of detection solutions for mutant *KRAS* gene at 0, 0.025, 0.05, 0.1, 0.2, 1.0, 5.0, and 50 nM. (C) Plot of absorbance versus DNA concentration. (D) Plot of absorbance versus logarithm of DNA concentration. (E) Photograph and (F) absorbance of detection solutions for marked sequences.

strategy. Similarly, with the increasing *let-7a* miR concentration, the color of the detection solution became bluer, the UV−vis spectra showed increased absorbance, and the plot of the absorbance versus *let-7a* miR concentration trended to a maximum value (Figure S6A−C). The absorbance depended linearly on the logarithm of DNA concentration ranging from 50 pM to 10 nM (R = 0.992, Figure S6D). The limit of detection (LOD) was estimated to be 21.7 pM. Thus, this nanozyme-catalyzed colorimetric strategy could conveniently be extended for miR detection.

The specificity of the proposed method for miR biosensing was examined with the *let-7* family, *let-7b*, *let-7c*, and *let-7d* miR and a negative control sequence. Only the target *let-7a* miR showed dramatic colorimetric response, whereas no obvious absorbance change was observed for the control, *let-7b*, and *let-7d* miR, and *let-7c* miR with a single-base mismatch showed slightly increased response (Figure S6E,F), indicating the good selectivity of this strategy for microRNA sensing.

We used *let-7a* miR to further demonstrate the designed signal amplification strategy. The control system contained *let-7a*, tHCR trigger, HCR H1, and HCR H2 (Table S1) for general HCR. Compared with the control HCR system, the tHCR strategy showed much lower background signal in the absence of *let-7a* miR (Figure 7A,B). When *let-7a* miR concentration reduced to 5 nM, the absorbance and the color of the detection solution for the HCR system were almost close to those of the blank (Figure 7B), suggesting relatively lower sensitivity. In contrast, when 5 nM *let-7a* miR was added to the tHCR system, the absorbance greatly increased (Figure 7A). Although the HCR system showed

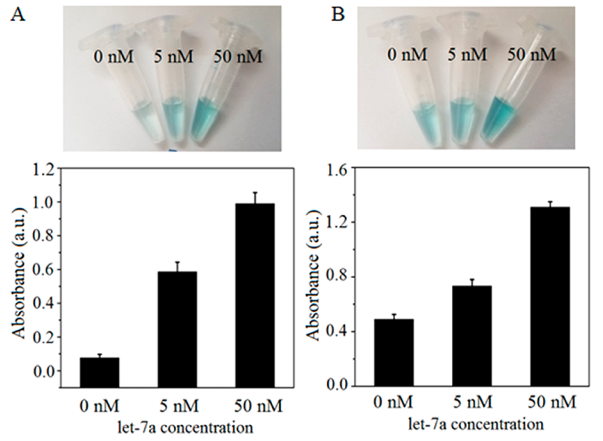

Figure 7. Photograph and absorbance of detection solutions for *let-7a* miR using (A) tHCR and (B) general HCR-based amplification.

higher absorbance than the tHCR system at the same miR concentration, which resulted from the absence of L3 and thus the decrease of DNA strands adsorbed on GO to hinder the deposition of PtNPs, the much higher background damaged its practicality. Therefore, the tHCR-based method achieved the amplified colorimetric assay.

CONCLUSION

This work designs a tHCR for accelerating the HCR and improving the specificity of target DNA-triggered assembly of DNA probes. When the target DNA-triggered tHCR and DNA-controlled growth of PtNPs on GO are integrated, a strategy to regulate the nanozyme activity is proposed for developing nanozyme-catalyzed colorimetric bioassays. The presence of linear-type DNA chain greatly improves the stability of the tHCR product and decreases the background. Thus, the developed colorimetric biosensing method shows excellent performance for amplified detection of both DNA and miR targets. The proposed strategy shows good extendability and can be integrated with different inorganic nanomaterials and used for detection of different target nucleic acids by changing the loop sequence of the tHCR trigger. Because of the binding of some proteins existing in clinical samples with a Pt-based precursor, appropriate separation of nucleic acids from some interference of proteins is needed when this strategy is used in biological and clinical fields.

ASSOCIATED CONTENT

Supporting Information

The Supporting Information is available free of charge at https://pubs.acs.org/doi/10.1021/acs.analchem.9b04909.

Sequence of used oligonucleotides, schematic illustration of DNA assembly through tHCR, SEM, and elemental mapping images of GO−PtNPs, DLS measurements and Raman spectra of GO−PtNPs and GO/DNA−PtNPs, gel electrophoresis of tHCR assembly, and performance comparison of self-assembled DNA−inorganic nanomaterials for colorimetric DNA sensing (PDF)

https://dx.doi.org/10.1021/acs.analchem.9b04909
Anal. Chem. 2020, 92, 2714−2721

AUTHOR INFORMATION

Corresponding Author

Huangxian Ju − *Nanjing University, Nanjing, P.R. China;* orcid.org/0000-0002-6741-5302; Phone: +86-25-89683593; Email: hxju@nju.edu.cn

Other Authors

Weiwei Chen − *Nanjing University, Nanjing, P.R. China*
Xiaobo Zhang − *Nanjing University, Nanjing, P.R. China*
Juanjuan Li − *Hainan Medical University, Haikou, P.R. China*
Lizhen Chen − *Nanjing University, Nanjing, P.R. China*
Ningning Wang − *Nanjing University, Nanjing, P.R. China*
Siqi Yu − *Nanjing University, Nanjing, P.R. China*
Guangming Li − *Nanjing University, Nanjing, P.R. China*
Linfei Xiong − *Nanjing University, Nanjing, P.R. China*

Complete contact information is available at: https://pubs.acs.org/10.1021/acs.analchem.9b04909

Notes

The authors declare no competing financial interest.

ACKNOWLEDGMENTS

We acknowledge the financial support of the National Natural Science Foundation of China (21635005 and 21361162002).

REFERENCES

(1) Wang, L. S.; Lei, J. P.; Ma, R. N.; Ju, H. X. *Anal. Chem.* **2013**, *85*, 6505−6510.
(2) Deng, H. H.; Lin, X. L.; Liu, Y. H.; Li, K. L.; Zhuang, Q. Q.; Peng, H. P.; Liu, A. L.; Xia, X. H.; Chen, W. *Nanoscale* **2017**, *9*, 10292−10300.
(3) Lei, J. P.; Ju, H. X. *Chem. Soc. Rev.* **2012**, *41*, 2122−2134.
(4) Song, S. P.; Qin, Y.; He, Y.; Huang, Q.; Fan, C. H.; Chen, H. Y. *Chem. Soc. Rev.* **2010**, *39*, 4234−4243.
(5) Roh, Y. H.; Ruiz, R. C. H.; Peng, S. M.; Lee, J. B.; Luo, D. *Chem. Soc. Rev.* **2011**, *40*, 5730−5744.
(6) Chen, Z. W.; Liu, C. Q.; Cao, F. F.; Ren, J. S.; Qu, X. G. *Chem. Soc. Rev.* **2018**, *47*, 4017−4072.
(7) Pei, H.; Li, F.; Wan, Y.; Wei, M.; Liu, H. J.; Su, Y.; Chen, N.; Huang, Q.; Fan, C. H. *J. Am. Chem. Soc.* **2012**, *134*, 11876−11879.
(8) Liu, B. W.; Sun, Z. Y.; Huang, P.-J. J.; Liu, J. W. *J. Am. Chem. Soc.* **2015**, *137*, 1290−1295.
(9) Liljeström, V.; Chen, C.; Dommersnes, P.; Fossum, J. O.; Gröschel, A. H. *Curr. Opin. Colloid Interface Sci.* **2019**, *40*, 25−41.
(10) Zhang, Q.; Huang, Y. H.; Wang, Y. M.; Li, S. H.; Jiang, Y. B. *Dyes Pigm.* **2019**, *169*, 111−117.
(11) Santiago-Rodríguez, L.; Sánchez-Pomales, G.; Cabrera, C. R. *Isr. J. Chem.* **2010**, *50*, 277−290.
(12) Lawal, A. T. *Biosens. Bioelectron.* **2019**, *141*, 111384.
(13) Lan, X.; Su, Z. M.; Zhou, Y. D.; Meyer, T.; Ke, Y. G.; Wang, Q. B.; Chiu, W.; Liu, N.; Zou, S. L.; Yan, H.; Liu, Y. *Angew. Chem., Int. Ed.* **2017**, *56*, 14632−14636.
(14) Wei, H.; Wang, E. K. *Chem. Soc. Rev.* **2013**, *42*, 6060−6093.
(15) Liang, S. M.; Yan, X. Y. *Acc. Chem. Res.* **2019**, *52*, 2190−2200.
(16) Chen, W. W.; Fang, X. E.; Ye, X.; Wang, X. J.; Kong, J. L. *Microchim. Acta* **2018**, *185*, 544.
(17) Wu, J. J.; Wang, X. Y.; Wang, Q.; Lou, Z. P.; Li, S. R.; Zhu, Y. Y.; Qin, L.; Wei, H. *Chem. Soc. Rev.* **2019**, *48*, 1004−1076.
(18) Chen, W. W.; Fang, X. E.; Li, H.; Cao, H. M.; Kong, J. L. *Biosens. Bioelectron.* **2017**, *94*, 169−175.
(19) Guo, Y. J.; Deng, L.; Li, J.; Guo, S. J.; Wang, E. K.; Dong, S. J. *ACS Nano* **2011**, *5*, 1282−1290.
(20) Liu, M.; Zhao, H. M.; Chen, S.; Yu, H. T.; Quan, X. *ACS Nano* **2012**, *6*, 3142−3151.
(21) Zheng, X. X.; Liu, Q.; Jing, C.; Li, Y.; Li, D.; Luo, W. J.; Wen, Y. Q.; He, Y.; Huang, Q.; Long, Y. T.; Fan, C. H. *Angew. Chem.* **2011**, *123*, 12200−12204.
(22) Jang, H. J.; Kim, Y. K.; Kwon, H. M.; Yeo, W. S.; Kim, D. E.; Min, D. H. *Angew. Chem., Int. Ed.* **2010**, *49*, 5703−5707.
(23) Balapanuru, J.; Yang, J. X.; Xiao, S.; Bao, Q. L.; Jahan, M.; Polavarapu, L.; Wei, J.; Xu, Q. H.; Loh, K. P. *Angew. Chem., Int. Ed.* **2010**, *49*, 6549−6553.
(24) Tao, Y.; Lin, Y. H.; Ren, J. S.; Qu, X. G. *Biomaterials* **2013**, *34*, 4810−4817.
(25) Bi, S.; Yue, S. Z.; Zhang, S. S. *Chem. Soc. Rev.* **2017**, *46*, 4281−4298.
(26) Chen, J. Y.; Tang, L. J.; Chu, X.; Jiang, J. H. *Analyst* **2017**, *142*, 3048−3061.
(27) Xiong, Y. Y.; Chen, Y. L.; Ding, L.; Liu, X. Q.; Ju, H. X. *Analyst* **2019**, *144*, 4545−4551.
(28) Xia, F.; White, R. J.; Zuo, X. L.; Patterson, A.; Xiao, Y.; Kang, D.; Gong, X.; Plaxco, K. W.; Heeger, A. J. *J. Am. Chem. Soc.* **2010**, *132*, 14346−14348.
(29) Huang, X.; Qi, X. Y.; Boey, F.; Zhang, H. *Chem. Soc. Rev.* **2012**, *41*, 666−686.
(30) Muschi, M.; Serre, C. *Coord. Chem. Rev.* **2019**, *387*, 262−272.
(31) Bharath, G.; Madhu, R.; Chen, S. M.; Veeramani, V.; Mangalaraj, D.; Ponpandian, N. *J. Mater. Chem. A* **2015**, *3*, 15529−15539.
(32) Tan, S. M.; Ambrosi, A.; Chua, C. K.; Pumera, M. *J. Mater. Chem. A* **2014**, *2*, 10668−10675.
(33) Zhang, J.; Dong, Y. H.; Zhu, W. F.; Xie, D.; Zhao, Y. L.; Yang, D. Y.; Li, M. *ACS Appl. Mater. Interfaces* **2019**, *11*, 18145−18152.
(34) Huo, M.; Li, S. Q.; Zhang, P. W.; Feng, Y. M.; Liu, Y. R.; Wu, N.; Ju, H. X.; Ding, L. *Anal. Chem.* **2019**, *91*, 3374−3381.